J. Mater. Chem. C

Supplementary Information

Synthesis, crystal structure, enhanced photoluminescent property and fluoride detection ability of S-heterocyclic annulated perylene diimide-polyhedral oligosilsesquioxane dye

Hai-Jie Ben,[1] Xiang-Kui Ren,*[,2] Bo Song,[4] Xiaopeng Li,[4] Yakai Feng,[2] Wei Jiang,[3] Er-Qiang Chen,[5] Zhaohui Wang,[3] Shichun Jiang,*[,1]

[1] School of Materials Science and Engineering, Tianjin University, Tianjin, 300350, P. R. China

[2] School of Chemical Engineering and Technology, Tianjin University, Tianjin, 300350, P. R. China

[3] Beijing National Laboratory for Molecular Science, Key Laboratory of Organic Solids, Institute of Chemistry, Chinese Academy of Sciences, Beijing 100190, P. R. China

[4] The Department of Chemistry, University of South Florida, 4202 East Fowler Avenue, Tampa, Florida 33620, United States

[5] Beijing National Laboratory for Molecular Sciences, College of Chemistry, Peking University, Beijing 100871, P. R. China

Fig. S1 ^{1}H NMR spectrum of **2a** recorded in $CDCl_3$.

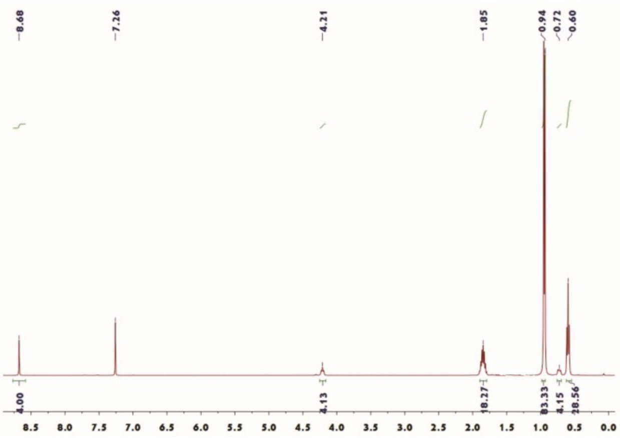

Fig. S2 ^{13}C NMR spectrum of **2a** recorded in $CDCl_3$.

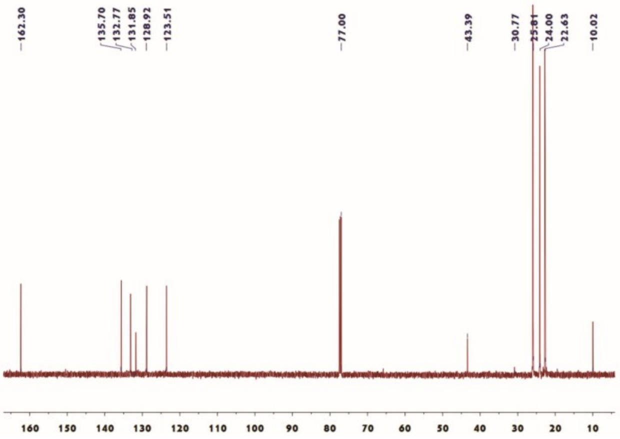

Fig. S3 ^{1}H NMR spectrum of POSS-SPDI-POSS recorded in $CDCl_3$.

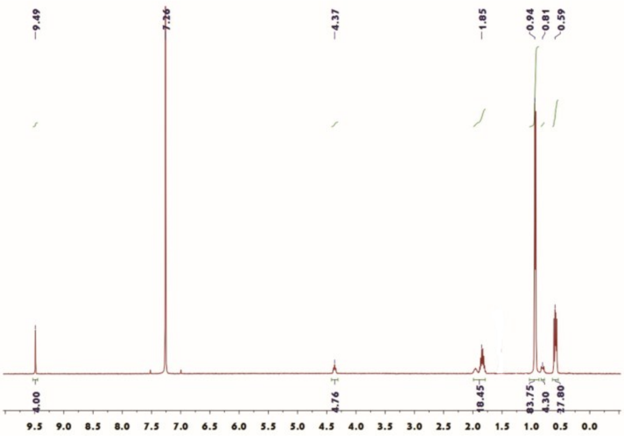

Fig. S4 ^{13}C NMR spectrum of POSS-SPDI-POSS recorded in CDCl$_3$.

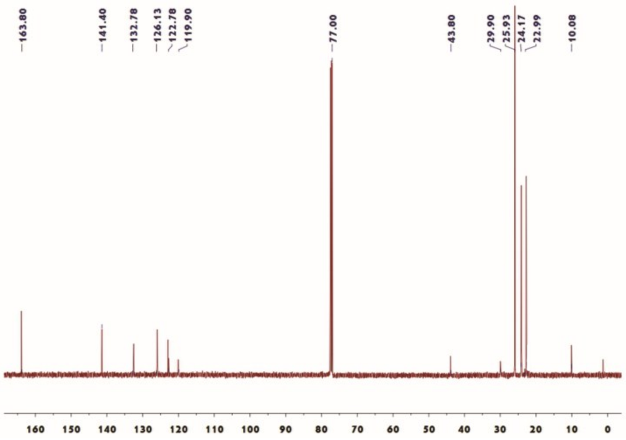

Fig. S5 FT-IR spectrum of POSS-SPDI-POSS compound.

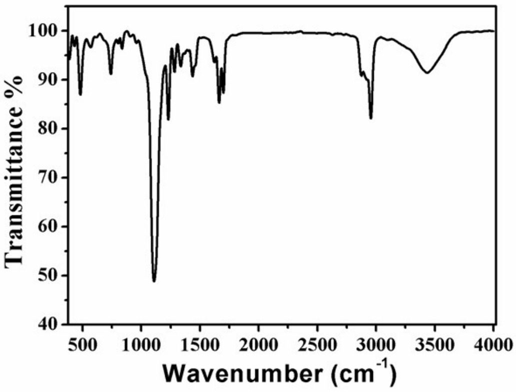

Fig. S6 ^{29}Si NMR spectrum of POSS-SPDI-POSS recorded in CDCl$_3$.

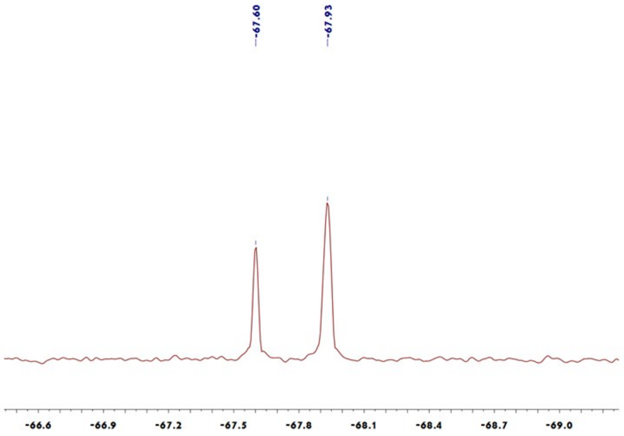

Fig. S7 Solvent-dependent UV/Vis spectra of (a) C8-SPDI-C8 and (b) POSS-SPDI-POSS in MCH/ $CHCl_3$ mixed solvent systems with different ratios from 1/1 to 5/1 in the concentration of 5×10^{-5} mol/L at 25 °C. Arrows indicate the changes upon increasing the addition of MCH.

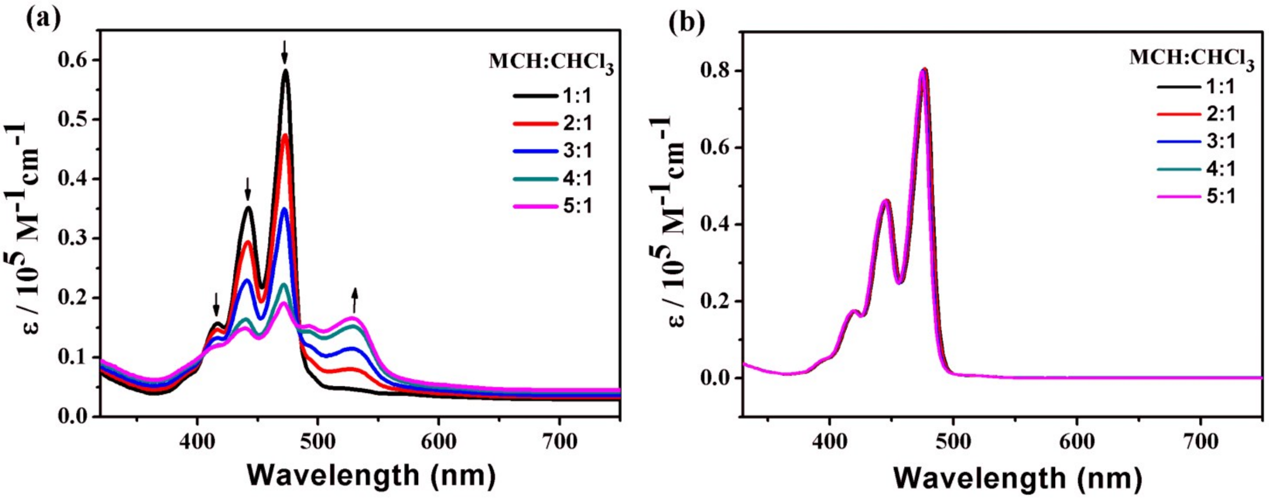

Fig. S8 Solvent-dependent UV/Vis spectra of branch-SPDI-branch in MeOH/ $CHCl_3$ mixed solvent systems with different ratios from 1/4 to 3/4 in the concentration of 5×10^{-5} mol/L at 25 °C.

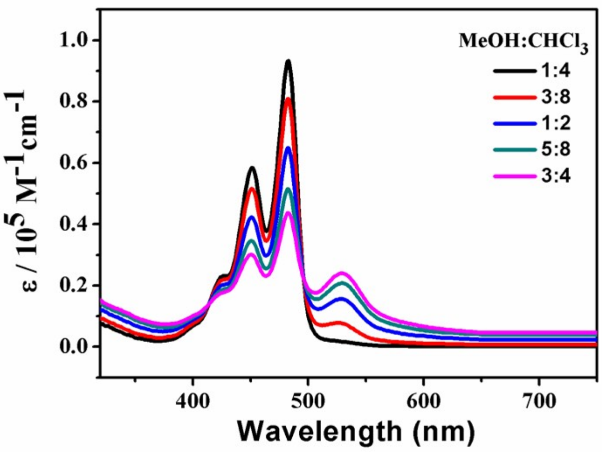

Fig. S9 TGA curve of the POSS-SPDI-POSS compound.

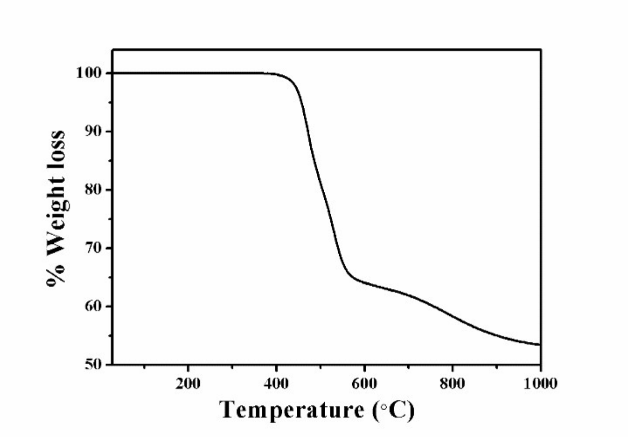

Fig. S10 A set of DSC cooling and subsequent heating thermal diagrams of POSS-SPDI-POSS (-10～350 °C) at a rate of 10 °C/min.

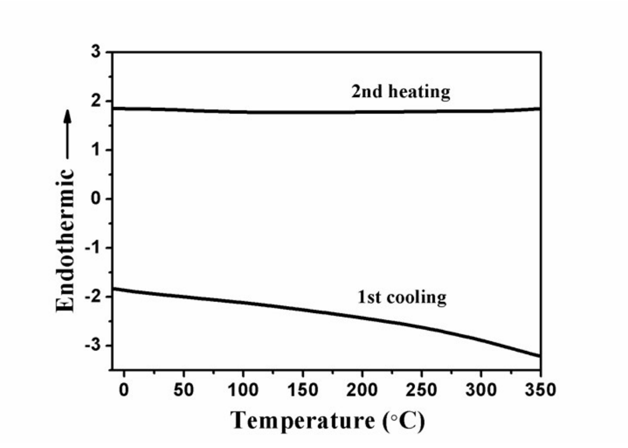

Fig. S11 1D SAXD pattern of C8-SPDI-C8.

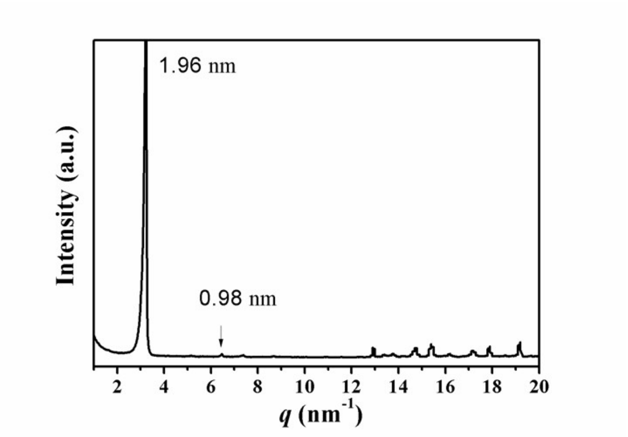

Fig. S12 2D WAXD pattern of the sheared C8-SPDI- C8.

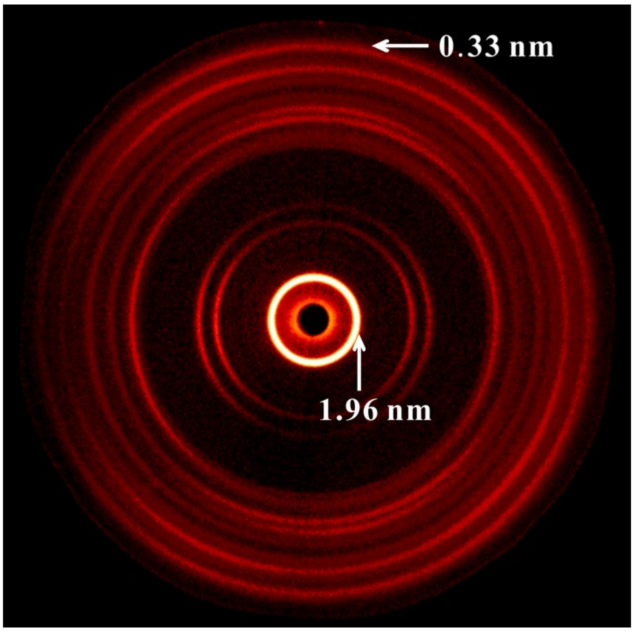

Fig. S13 Fluorescence emission change of C8-SPDI-C8 (30 μM in THF) observed upon the addition of various anions (300 μM). Inset: the optical changes in fluorescence emission and color by UV irradiation (naked-eye detection).

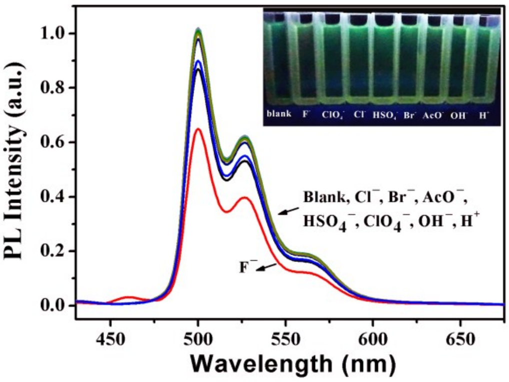

Fig. S14 Bar graphs of fluorescence intensity change of (a) C8-SPDI-C8 (30 μM in THF) and (b) POSS-SPDI-POSS (30 μM in THF) observed upon the addition of various anions (300 μM). "F/F_0" represents the final fluorescence intensity/initial fluorescence intensity.

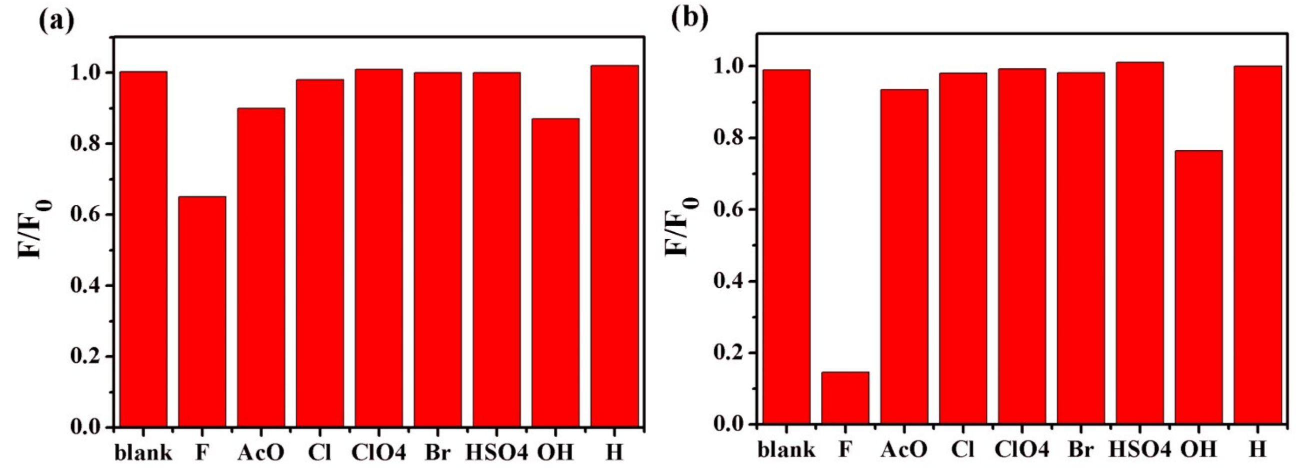

Fig. S15 (a) ^{1}H NMR spectra (ranged 4.5-12 ppm) of POSS-SPDI-POSS in $CDCl_3$ (upper) and the solute after the addition of 10 equiv TBAF (below). (b) ^{1}H NMR spectra (ranged 0.4-3 ppm) of POSS-SPDI-POSS in $CDCl_3$ (upper) and the solute after the addition of 10 equiv TBAF (below). (The mark * is ascribed to the CH_3-$CH(CH_3)$-CH_2^- ion which comes from the isobutyl group of POSS cloven by fluoride). (c) ^{19}F NMR spectra of TBAF in $CDCl_3$ (upper) and the solute after the addition of 10 equiv TBAF (below) in $CDCl_3$. (d) ^{29}Si NMR spectra of POSS-SPDI-POSS in $CDCl_3$ (upper) and the solute after the addition of 10 equiv TBAF (below) in $CDCl_3$. (The POSS-SPDI POSS was dissolved 30 μM in THF; upon addition of 10 equiv TBAF in the solution, the THF solvent was removed under vacuum. Then the solute was dissolved in $CDCl_3$ for the ^{1}H NMR experiment, ^{19}F NMR and ^{29}Si NMR.)

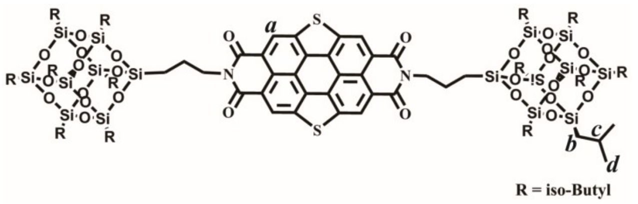

(a)

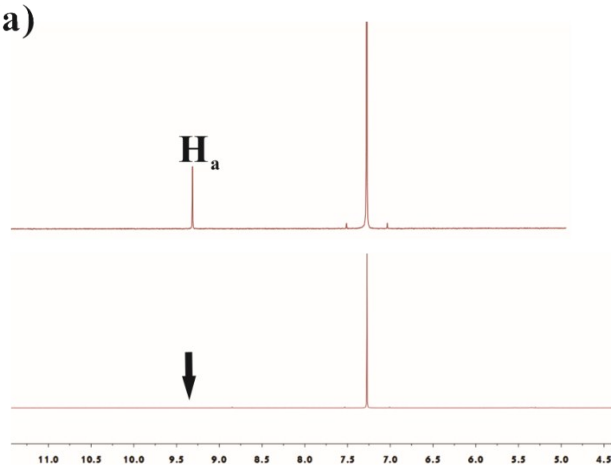
H_a
11.0
10.5
10.0
9.5
9.0
8.5
8.0
7.5
7.0
6.5
6.0
5.5
5.0
4.5

(b)

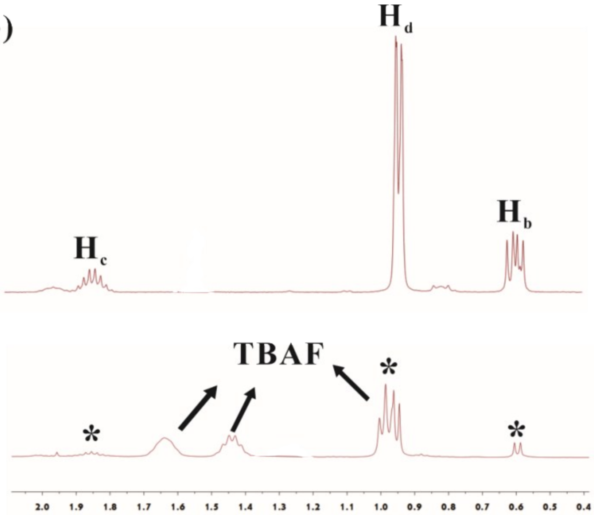
H_d
H_c
H_b
TBAF
*
*
*
2.0
1.9
1.8
1.7
1.6
1.5
1.4
1.3
1.2
1.1
1.0
0.9
0.8
0.7
0.6
0.5
0.4

(c)

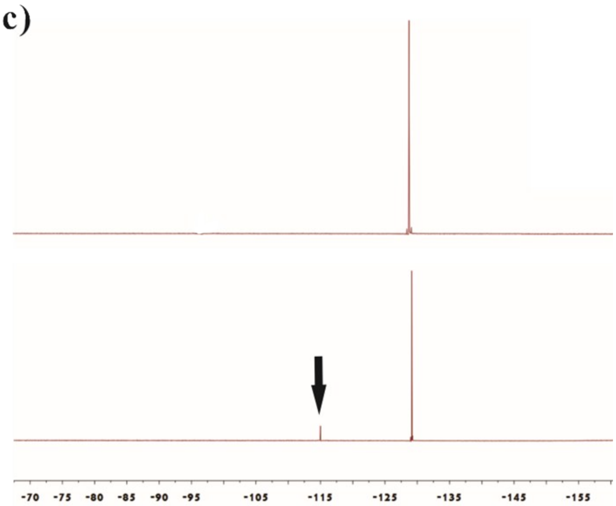
-70
-75
-80
-85
-90
-95
-105
-115
-125
-135
-145
-155

(d)

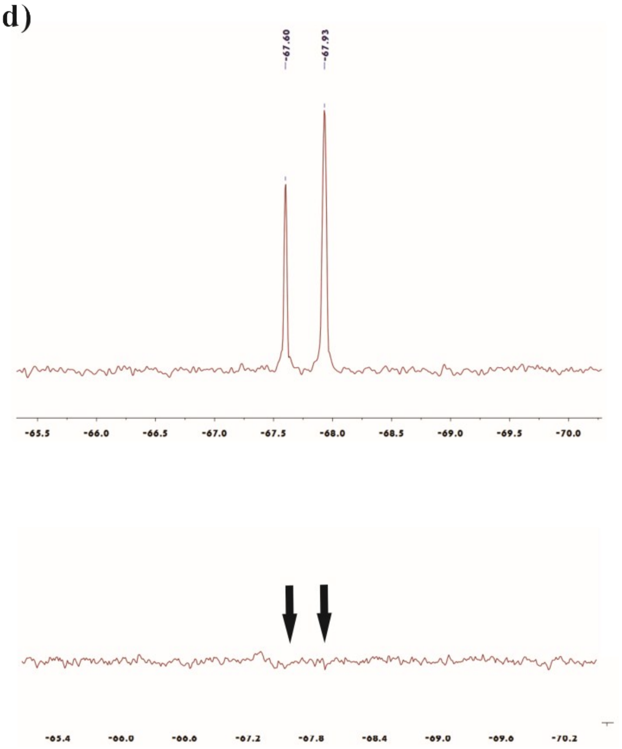

Table S1 Experimental and calculated crystallographic parameters of POSS-SPDI-POSS.

	2θ (deg)		*d*-spacing (nm)		Intensity
(*hkl*)	expt[a]	calcd[b]	expt[a]	calcd[b]	expt[c]
100	3.75	3.75	2.36	2.36	vw
010	4.07	4.07	2.17	2.17	vs
-110	5.41	5.41	1.63	1.63	s
200	7.50	7.50	1.18	1.18	vw
020	8.16	8.14	1.08	1.09	vs
210	8.78	8.70	1.01	1.02	vs
-220	10.83	10.83	0.82	0.82	w
310	12.12	12.15	0.73	0.73	w
130	12.93	12.96	0.68	0.68	vw
-320	13.70	13.61	0.65	0.65	vw
-330	16.40	16.28	0.54	0.54	vw
340	20.30	20.30	0.44	0.44	m
520	21.10	20.88	0.42	0.43	w
001	8.00	8.00	1.11	1.11	vs
111	10.10	9.80	0.88	0.90	s
211	11.90	11.83	0.74	0.75	m
-221	13.50	13.48	0.66	0.66	vw
-321	15.70	15.81	0.56	0.56	vw
-231	16.50	16.21	0.54	0.55	vw
-331	18.40	18.16	0.48	0.49	w
002	16.00	16.04	0.55	0.55	w
-112	17.30	16.94	0.51	0.52	w
212	18.50	18.27	0.48	0.49	m
-332	23.10	22.93	0.39	0.39	vw
003	24.10	24.16	0.37	0.37	vw

[a] Experimental values observed in Fig. 6. [b] Calculated values based on the monoclinic unit cell of a = 2.36 nm, b = 2.17 nm, c = 1.11 nm, $\alpha = \beta$ = 90°, γ = 92.57°. [c] The experimental intensities in Fig. 6 are semiquantitatively estimated via amicrodesitometer and classified as very strong (vs), strong (s), medium (m), weak (w), and very weak (vw).